Draft version July 1, 2020
Typeset using LaTeX **twocolumn** style in AASTeX63

Spin Dynamics in Hierarchical Black Hole Triples: Predicting Final Spin-Orbit Misalignment Angle From Initial Conditions

Yubo Su,[1] Dong Lai,[1] and Bin Liu

[1] *Cornell Center for Astrophysics and Planetary Science, Department of Astronomy, Cornell University, Ithaca, NY 14853, USA*

(Received XXXX; Revised XXXX; Accepted XXXX)

Submitted to ApJL

ABSTRACT

Abstract

Keywords: keywords

1. INTRODUCTION

This problem is important.

In Section 2, we set up the relevant equations of motion for the orbital and spin evolution of the three BHs, and we argue for the primary result of the paper, conservation of the angle θ_e. In Sections 3 and 4, we consider two scenarios under which conservation of θ_e can be violated. We discuss and conclude in Section 5.

2. ANALYTICAL SETUP

2.1. *Orbital Evolution*

We study Lidov-Kozai (LK) oscillations due to an external perturber to quadrupole order and include precession of pericenter and gravitational wave radiation due to general relativity. Consider an inner black hole (BH) binary with masses m_1 and m_2 having total mass m_{12} and reduced mass μ orbited by a third BH with mass m_3. Call a_3 the orbital semimajor axis of the third BH from the center of mass of the inner binary, and e_3 the eccentricity of its orbit, and define effective semimajor axis

$$\tilde{a}_3 \equiv a_3\sqrt{1-e_3^2}. \tag{1}$$

For simplicity, we adopt the test particle approximation such that the orbit of the third mass is fixed[1]. Call $\mathbf{L}_{\rm out} \equiv L_{\rm out}\hat{\mathbf{L}}_{\rm out}$ the fixed angular momentum of the outer BH relative to the center of mass of the inner BH binary, and call $\mathbf{L} \equiv L\hat{\mathbf{L}}$ the orbital angular momentum of the inner BH binary.

Corresponding author: Yubo Su
yubosu@astro.cornell.edu

[1] At quadrupole order, including the back-reaction terms is equivalent to considering LK oscillations of the inner binary about a fixed total angular momentum axis rather than $\mathbf{L}_{\rm out}$ (see e.g. Liu & Lai 2017, 2018).

We then consider the motion of the inner binary, described by orbital elements Keplerian orbital elements $(a, e, \Omega, I, \omega)$. The equations describing the motion of these orbital elements are (Peters 1964; Storch & Lai 2015; Liu & Lai 2018)

$$\frac{{\rm d}a}{{\rm d}t} = \left(\frac{{\rm d}a}{{\rm d}t}\right)_{\rm GW}, \tag{2}$$

$$\frac{{\rm d}e}{{\rm d}t} = \frac{15}{8t_{\rm LK}}e\sqrt{1-e^2}\sin 2\omega\sin^2 I + \left(\frac{{\rm d}e}{{\rm d}t}\right)_{\rm GW}, \tag{3}$$

$$\frac{{\rm d}\Omega}{{\rm d}t} = \frac{3}{4t_{\rm LK}}\frac{\cos I\left(5e^2\cos^2\omega - 4e^2 - 1\right)}{\sqrt{1-e^2}} + \Omega_{\rm GR}, \tag{4}$$

$$\frac{{\rm d}I}{{\rm d}t} = \frac{15}{16}\frac{e^2\sin 2\omega\sin 2I}{\sqrt{1-e^2}}, \tag{5}$$

$$\frac{{\rm d}\omega}{{\rm d}t} = \frac{3}{4t_{\rm LK}}\frac{2\left(1-e^2\right) + 5\sin^2\omega(e^2 - \sin^2 I)}{\sqrt{1-e^2}}, \tag{6}$$

where we define

$$t_{\rm LK}^{-1} = n\left(\frac{m_3}{m_{12}}\right)\left(\frac{a}{\tilde{a}_3}\right)^3, \tag{7}$$

$$\left(\frac{{\rm d}a}{{\rm d}t}\right)_{\rm GW} = -\frac{a}{t_{\rm GW}}, \tag{8}$$

$$= \frac{64}{5}\frac{G^3\mu m_{12}^2}{c^5a^3}\frac{1}{\left(1-e^2\right)^{7/2}}\left(1 + \frac{73}{24}e^2 + \frac{37}{96}e^4\right), \tag{9}$$

$$\left(\frac{{\rm d}e}{{\rm d}t}\right)_{\rm GW} = -\frac{304}{15}\frac{G^3\mu m_{12}^2}{c^5a^4}\frac{1}{\left(1-e^2\right)^{5/2}}\left(1 + \frac{121}{304}e^2\right), \tag{10}$$

$$\Omega_{\rm GR} = \frac{3Gnm_{12}}{c^2a\left(1-e^2\right)}, \tag{11}$$

and $n = \sqrt{Gm_{12}/a^3}$ is the mean motion of the inner binary. We will often refer to $e_{\rm min}$ and $e_{\rm max}$ the minimum/maximum

a	0.1 AU	100 AU
$\tilde{a}_3$	3 AU	4500 AU
m_{12}	$60M_\odot$	$50M_\odot$
m_3	$30M_\odot$	$30M_\odot$
e_0	0.001	0.001

Table 1. Shown are the primary two sets of parameters considered in the numerical simulations of this paper. We will refer to the first configuration as the "close-in" configuration. Parameters not shown here are varied between simulations and are described in line.

eccentricity in a single LK cycle, and we will sometimes notate $j = \sqrt{1-e^2}$ and $j_{\rm min} = \sqrt{1-e^2_{\rm max}}$.

Finally, for concreteness, numerical simulations use parameters similar those considered in Liu & Lai (2017, 2018), given in Table 1, though our theory is general.

2.2. *Spin Dynamics: $\theta_{\rm e}$ as an Adiabatic Invariant*

We are ultimately interested in the spin orientations of the inner BHs at merger as a function of initial conditions. Since they evolve independently to leading post-Newtonian order, we focus on the dynamics of a single BH spin vector $\mathbf{S} = S\hat{\mathbf{S}}$. Neglecting spin-spin interactions, $\hat{\mathbf{S}}$ undergoes de Sitter precession about $\mathbf{L}$ as

$$\frac{{\rm d}\hat{\mathbf{S}}}{{\rm d}t} = \Omega_{\rm SL}\hat{\mathbf{L}}\times\hat{\mathbf{S}}, \tag{12}$$

$$\Omega_{\rm SL} = \frac{3Gn\left(m_2+\mu/3\right)}{2c^2a\left(1-e^2\right)}. \tag{13}$$

To analyze the dynamics of the spin vector, we go to co-rotating frame with $\hat{\mathbf{L}}$ about $\hat{\mathbf{L}}_{\rm out}$. Choose $\hat{\mathbf{L}}_{\rm out} = \hat{\mathbf{z}}$, and choose the $\hat{\mathbf{x}}$ axis such that $\hat{\mathbf{L}}$ lies in the x-z plane. In this coordinate system, Eq. (12) becomes

$$\left(\frac{{\rm d}\mathbf{S}}{{\rm d}t}\right)_{\rm rot} = \left(-\frac{{\rm d}\Omega}{{\rm d}t}\hat{\mathbf{z}} + \Omega_{\rm SL}\hat{\mathbf{L}}\right)\times\hat{\mathbf{S}}, \tag{14}$$

$$= \boldsymbol{\Omega}_{\rm e}\times\hat{\mathbf{S}}, \tag{15}$$

$$\boldsymbol{\Omega}_{\rm e} \equiv \Omega_{\rm L}\hat{\mathbf{z}} + \Omega_{\rm SL}\left(\cos I\hat{\mathbf{z}} + \sin I\hat{\mathbf{x}}\right), \tag{16}$$

$$\Omega_{\rm L} \equiv -\frac{{\rm d}\Omega}{{\rm d}t}. \tag{17}$$

In general, Eq. (15) is difficult to analyze, since $\Omega_{\rm L}$, $\Omega_{\rm SL}$ and I all vary significantly within each LK period, and we are interested in the final outcome after many LK periods. However, if we assume $t_{\rm GW} \gg t_{\rm LK}$, then the system can be treated as nearly periodic within each LK cycle. We can then rewrite Eq. (15) in Fourier components

$$\left(\frac{{\rm d}\hat{\mathbf{S}}}{{\rm d}t}\right)_{\rm rot} = \left[\overline{\boldsymbol{\Omega}}_{\rm e} + \sum_{N=1}^{\infty}\boldsymbol{\Omega}_{\rm e,N}\cos\left(\frac{2\pi Nt}{T_{\rm LK}}\right)\right]\times\hat{\mathbf{S}}. \tag{18}$$

The bar denotes an average over an LK cycle. We adopt convention where $t = 0$ is the maximum eccentricity phase of the LK cycle.

We next assume that the $N \geq 1$ harmonics vanish when the equation of motion is averaged over an LK cycle (this is not always correct, and one scenario in which this assumption fails is analyzed in Section 4). This gives

$$\left(\frac{{\rm d}\hat{\bar{\mathbf{S}}}}{{\rm d}t}\right)_{\rm rot} = \overline{\boldsymbol{\Omega}}_{\rm e}\times\hat{\bar{\mathbf{S}}}. \tag{19}$$

Eq. (19) suggests that $\theta_{\rm e}$, given by

$$\cos\theta_{\rm e} \equiv \hat{\bar{\mathbf{S}}}\cdot\hat{\overline{\boldsymbol{\Omega}}}_{\rm e}, \tag{20}$$

should be a conserved quantity when $\boldsymbol{\Omega}_{\rm e}$ varies adiabatically. The adiabaticity condition requires the precession axis evolve slowly compared to the precession frequency at all times:

$$\left|\frac{{\rm d}\hat{\overline{\boldsymbol{\Omega}}}_{\rm e}}{{\rm d}t}\right| \ll \left|\overline{\boldsymbol{\Omega}}_{\rm e}\right|. \tag{21}$$

Since the orientation of $\overline{\boldsymbol{\Omega}}_{\rm e}$ changes on timescale $t_{\rm GW}$, we see that the adiabatic assumption is roughly equivalent to assuming each LK period can be Fourier decomposed [Eq. (18)].

To be more precise, we define an inclination angle $I_{\rm e}$ for $\overline{\boldsymbol{\Omega}}_{\rm e}$ as shown in Fig. 2. Denoting also $\overline{\Omega}_{\rm e} \equiv \left|\overline{\boldsymbol{\Omega}}_{\rm e}\right|$, the adiabaticity condition can be expressed as

$$\frac{{\rm d}I_{\rm e}}{{\rm d}t} \ll \overline{\Omega}_{\rm e}. \tag{22}$$

Next, we express $I_{\rm e}$ in closed form. When the eccentricity is strongly oscillatory within each LK cycle (early in the evolution, see Fig. 1), we define averaged quantities

$$\overline{\Omega_{\rm SL}\sin I} \equiv \overline{\Omega}_{\rm SL}\sin\bar{I}, \tag{23}$$

$$\overline{\Omega_{\rm SL}\cos I} \equiv \overline{\Omega}_{\rm SL}\cos\bar{I}. \tag{24}$$

Then, using Eq.(16), we can see that

$$\tan I_{\rm e} = \frac{\bar{\mathcal{A}}\sin\bar{I}}{1+\bar{\mathcal{A}}\cos\bar{I}}, \tag{25}$$

where

$$\bar{\mathcal{A}} \equiv \frac{\overline{\Omega}_{\rm SL}}{\overline{\Omega}_{\rm L}}. \tag{26}$$

When eccentricity oscillations are suppressed (at later times, see Fig. 1), we just have $\overline{\Omega}_{\rm SL} = \Omega_{\rm SL}$, $\overline{\Omega}_{\rm L} = \Omega_{\rm L}$, and $\bar{I} = I$.

3. ANALYSIS: DEVIATION FROM ADIABATICITY

In real systems, the particular extent to which $\theta_{\rm e}$ is conserved depends on how well Eq. (21) is satisfied. We will first present equations of motion for $\theta_{\rm e}$. We will then derive accurate estimates for important quantities in these equations of motion, and use these estimates to derive upper bounds on $\Delta\theta_{\rm e}$, the change in $\theta_{\rm e}$ over the entire inspiral. Taken together, this calculation estimates the deviation from adiabaticity as a function of initial conditions.

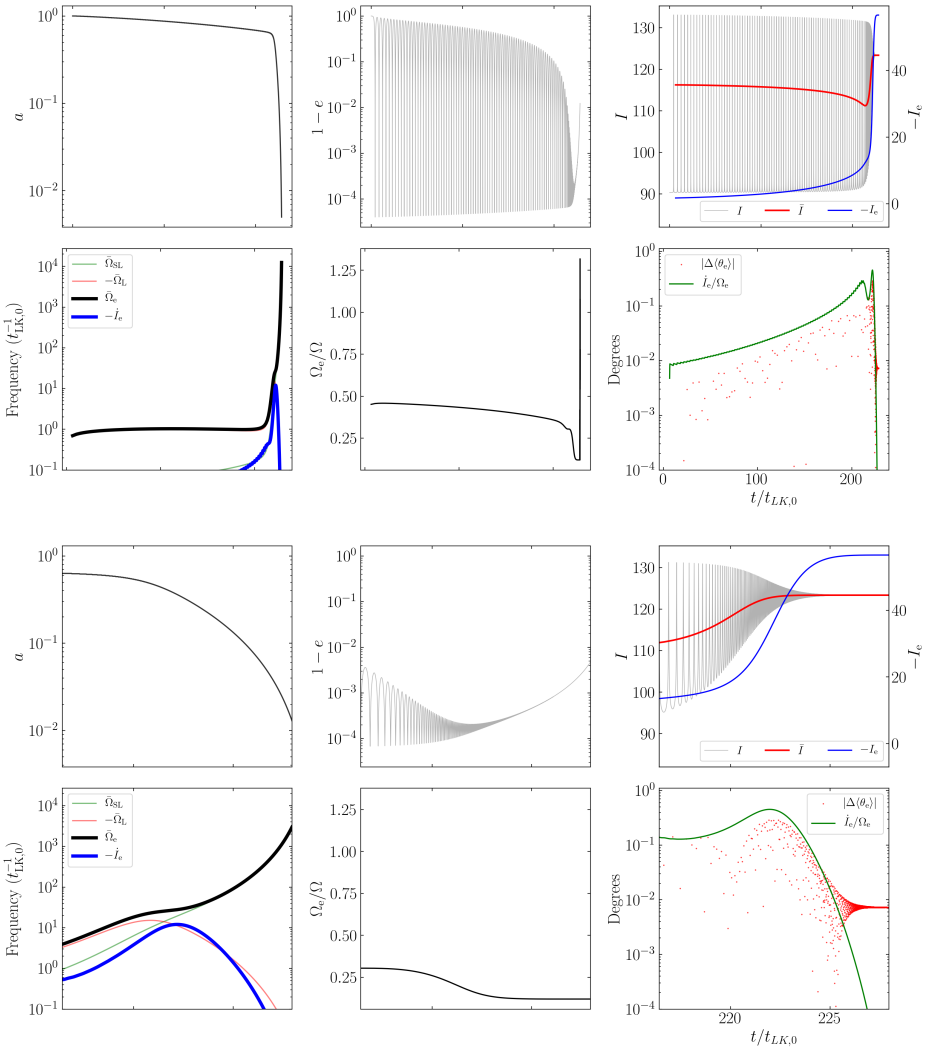

Figure 1. Plot.

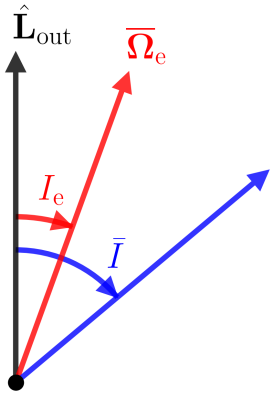

Figure 2. Definition of angles, shown in plane of the two angular momenta $\mathbf{L}_{\rm out}$ and $\mathbf{L}$, or the $\hat{\mathbf{x}}$–$\hat{\mathbf{z}}$ plane in the corotating frame. Note that for $I > 90°$, $I_{\rm e} < 0$.

3.1. *Equation of Motion*

From the corotating frame [Eq. (19)], consider going to the reference frame where $\hat{\mathbf{z}} = \hat{\bar{\mathbf{\Omega}}}_{\rm e}$ by rotation $-\dot{I}_{\rm e}\hat{\mathbf{y}}$. In this reference frame, the polar coordinate is just $\theta_{\rm e}$ as defined above in Eq. (20), and we call the azimuthal coordinate $\phi_{\rm e}$. In this reference frame, the equation of motion becomes

$$\left(\frac{{\rm d}\hat{\mathbf{S}}}{{\rm d}t}\right)' = \hat{\bar{\mathbf{\Omega}}}_{\rm e} \times \hat{\mathbf{S}} - \dot{I}_{\rm e}\hat{\mathbf{y}} \times \hat{\mathbf{S}}. \tag{27}$$

If we break $\hat{\mathbf{S}}$ into components $\hat{\mathbf{S}} = S_x\hat{\mathbf{x}} + S_y\hat{\mathbf{y}} + \cos\theta_{\rm e}\hat{\mathbf{z}}$ and define complex variable

$$S_\perp \equiv S_x + iS_y = \sin\theta e^{i\phi_{\rm e}}, \tag{28}$$

we can rewrite Eq. 27 as

$$\frac{{\rm d}S_\perp}{{\rm d}t} = i\left(\bar{\Omega}_{\rm e}\right) S_\perp - \dot{I}_{\rm e}\cos\theta_{\rm e}. \tag{29}$$

Defining

$$\Phi(t) = \int^t \bar{\Omega}_{\rm e}\, {\rm d}t, \tag{30}$$

we obtain formal solution

$$e^{-i\Phi}\left[S_\perp(t=\infty)-S_\perp(t=-\infty)\right]=-\int_{-\infty}^{\infty}e^{-i\Phi(\tau)}\dot{I}_{\rm e}\cos\theta\,{\rm d}\tau. \tag{31}$$

It can be seen that, in the adiabatic limit [Eq. (22)], $|S_\perp|$ (and therefore $\theta_{\rm e}$) is conserved, as the phase of the integrand in the right hand side varies much faster than the magnitude. Furthermore, the deviation from exact conservation of $|S_\perp|$ cannot exceed $\dot{I}_{\rm e}/\overline{\Omega}_{\rm e}$ so long as $\dot{I}_{\rm e}\lesssim\overline{\Omega}_{\rm e}$[2]. In the following section, we show that this maximum value can be calculated to good accuracy from initial conditions.

3.2. *Estimate of Deviation from Adiabaticity*

Towards estimating the maximum $\dot{I}_{\rm e}/\overline{\Omega}_{\rm e}$, we first differentiate Eq. (25),

$$\dot{\bar{I}}_{\rm e}=\left(\frac{\dot{\bar{\mathcal{A}}}}{\bar{\mathcal{A}}}\right)\frac{\bar{\mathcal{A}}\sin\bar{I}}{1+2\bar{\mathcal{A}}\cos\bar{I}+\bar{\mathcal{A}}^2}. \tag{32}$$

It can be easily shown from Eq. (16) that

$$\overline{\Omega}_{\rm e}=\overline{\Omega}_{\rm L}\left(1+2\bar{\mathcal{A}}\cos\bar{I}+\bar{A}^2\right)^{1/2}, \tag{33}$$

from which we obtain

$$\left|\frac{\dot{\bar{I}}_{\rm e}}{\overline{\Omega}_{\rm e}}\right|=\left|\frac{\dot{\bar{\mathcal{A}}}}{\bar{\mathcal{A}}}\right|\frac{1}{\left|\overline{\Omega}_{\rm L}\right|}\frac{\bar{\mathcal{A}}\sin\bar{I}}{\left(1+2\bar{\mathcal{A}}\cos\bar{I}+\bar{\mathcal{A}}\right)^{3/2}}. \tag{34}$$

This is maximized when $\bar{\mathcal{A}}\simeq 1$, and so we obtain that the maximum deviation should be bounded by

$$\left|\frac{\dot{I}_{\rm e}}{\overline{\Omega}_{\rm e}}\right|_{\rm max}\simeq\left|\frac{\dot{\bar{\mathcal{A}}}}{\bar{\mathcal{A}}}\right|\frac{1}{\left|\overline{\Omega}_{\rm L}\right|}\frac{\sin\bar{I}}{\left(2+2\cos\bar{I}\right)^{3/2}}. \tag{35}$$

To evaluate this, we make two assumptions: (i) $\bar{I}$ is approximately constant, and (ii) $j_{\rm min}=\sqrt{1-e_{\rm max}^2}$ evaluated at $\bar{\mathcal{A}}\simeq 1$ is some constant multiple of the initial $j_{\rm min}$, so that

$$j_\star\equiv(j)_{\bar{\mathcal{A}}\simeq 1}=f\sqrt{\frac{5}{3}\cos^2 I_0}, \tag{36}$$

for some unknown factor $f>1$; we use star subscripts to denote evaluation at $\bar{\mathcal{A}}\simeq 1$. f turns out to be relatively insensitive to I_0. This can be as systems with lower $e_{\rm max}$ values take more cycles to attain $\bar{\mathcal{A}}\simeq 1$ and thus experience a similar amount of decay due to GW radiation.

[2] Given the complicated evolution of $\overline{\Omega}_{\rm e}$ and $\dot{I}_{\rm e}$, it is difficult to give a more exact bound on the deviation from adiabaticity. In practice, deviations $\lesssim 1^\circ$ are observationally indistinguishable, so the exact scaling in this regime is negligible.

For simplicity, let's first assume $\bar{\mathcal{A}}\simeq 1$ is satisfied when the LK oscillations are mostly suppressed, and $e_\star\approx 1$ throughout the LK cycle (we will later see that the scalings are the same in the LK-oscillating regime). Then we can write

$$\bar{\mathcal{A}}\simeq\frac{3Gn\,(m_2+\mu/3)}{2c^2aj^2}\left[\frac{3\cos\bar{I}}{4t_{\rm LK}}\frac{1+3e^2/2}{j}\right]^{-1}, \tag{37}$$

$$\simeq\frac{G(m_2+\mu/3)m_{12}\tilde{a}_3^3}{c^2m_3a^4j\cos\bar{I}}, \tag{38}$$

$$\propto\frac{1}{a^4j}, \tag{39}$$

$$\frac{\dot{\bar{\mathcal{A}}}}{\bar{\mathcal{A}}}=-4\left(\frac{\dot{a}}{a}\right)_{\rm GW}+\frac{e}{j^2}\left(\frac{{\rm d}e}{{\rm d}t}\right)_{\rm GW}. \tag{40}$$

Approximating $e_\star\approx 1$ in Eqs. (9) and (10) gives

$$\left[\frac{\dot{\bar{\mathcal{A}}}}{\bar{\mathcal{A}}}\right]_{\bar{\mathcal{A}}=1}\simeq\frac{64G^3\mu m_{12}^2}{5c^5a_\star^4j_\star^7}\times 15, \tag{41}$$

$$\overline{\Omega}_{{\rm L},\star}\approx\frac{3\cos\bar{I}}{2t_{\rm LK}j_\star}, \tag{42}$$

$$\left|\frac{\dot{\bar{I}}_{\rm e}}{\overline{\Omega}_{\rm e}}\right|_{\rm max}\approx\frac{128G^3\mu m_{12}^2}{c^5a_\star^4j_\star^6}\frac{t_{\rm LK}}{\cos\bar{I}}\frac{\sin\bar{I}}{\left(2+2\cos\bar{I}\right)^{3/2}}. \tag{43}$$

With the ansatz for $j_\star$ given by Eq. (36) and requiring Eq. (38) equal 1 for a given $j_\star$ and $a_\star$ gives us the final expression

$$\left|\frac{\dot{\bar{I}}_{\rm e}}{\overline{\Omega}_{\rm e}}\right|_{\rm max}\approx\frac{128G^3\mu m_{12}^3\tilde{a}_3^3}{c^5\sqrt{Gm_{12}}m_3}\left(\frac{c^2m_3\cos\bar{I}}{G(m_2+\mu/3)m_{12}\tilde{a}_3^3}\right)^{11/8}\times(j_\star)^{-37/8}\frac{\tan\bar{I}}{\left(2+2\cos\bar{I}\right)^{3/2}}. \tag{44}$$

The agreement of Eq. (44) with numerical simulation is remarkable, as shown in Fig. 3.

Above, we assumed that $\bar{\mathcal{A}}\simeq 1$ is satisfied when the eccentricity is mostly constant (see Fig. 1 for an indication of how accurate this is for the parameter space explored in Fig. 3). It is also possible that $\bar{\mathcal{A}}\simeq 1$ occurs when the eccentricity is still undergoing substantial oscillations. Surprisingly, Eq. (44) is still accurate in this regime by just replacing e with $e_{\rm max}$. When $e_{\rm min}\ll e_{\rm max}$, the binary spends a fraction $\sim j_{\rm min}$ of the LK cycle near $e\simeq e_{\rm max}$ (Anderson et al. 2016). This fraction of the LK cycle dominates both GW dissipation and $\overline{\Omega}_{\rm L}$ precession. Thus, both $\dot{\bar{\mathcal{A}}}$ and $\overline{\Omega}_{\rm L}$ in Eq. (35) are evaluated at $e\approx e_{\rm max}$ and are suppressed by a factor of $j_{\rm min}$. The $j_{\rm min}$ suppression factors cancel out in Eq. (44), and so when the eccentricity is still substantially oscillating, Eq. (44) remains accurate when e is replaced with $e_{\rm max}$.

The accuracy of Eq. (44) in bounding the total change in $\Delta\theta_{\rm e}$ over inspiral is shown in Fig. 4. Note that conservation of $\Delta\theta_{\rm e}$

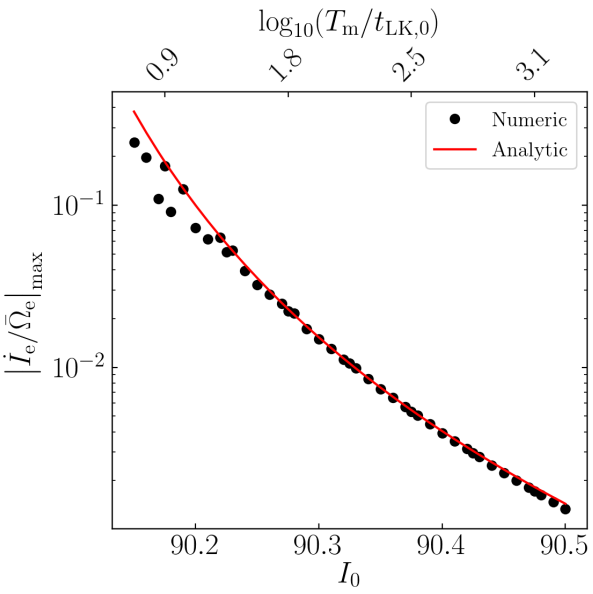

Figure 3. Comparison of $\left|\dot{\bar{I}}_e/\bar{\Omega}_e\right|_{max}$ extracted from simulations and using Eq. (44), where we take $f = 2.6$ in Eq. (36). The merger time T_m is shown along the top axis of the plot in units of the characteristic LK timescale at the start of inspiral $t_{LK,0}$; the LK period is initially of order a few $t_{LK,0}$. The agreement is remarkable for mergers that are more adiabatic (towards the right).

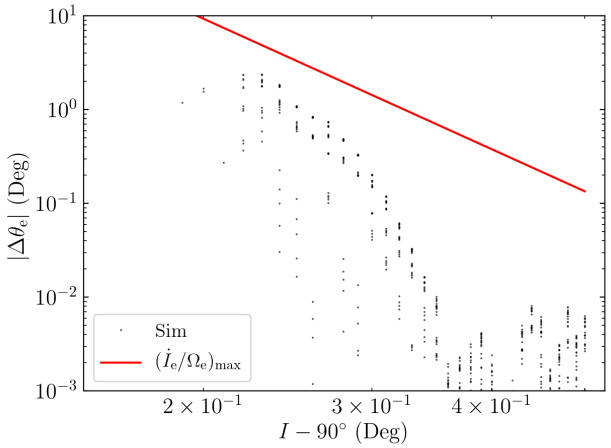

Figure 4. Change in θ_e over inspiral as a function of initial inclination I_0. Plotted for comparison is the bound $\Delta\theta_e \lesssim \left|\dot{\bar{I}}_e/\bar{\Omega}_e\right|_{max}$, given by Eq. (44). It is clear that the given bound is not tight but provides an upper bound for non-conservation of θ_e due to nonadiabatic effects. The leftmost portion of this plot is less reliable as the quasi-periodic assumption within each LK cycle breaks down as GW dissipation within each LK cycle is substantial.

is generally much better than Eq. (44) predicts; cancellation of phases in Eq. (31) is generally more efficient than assumed in this bound.

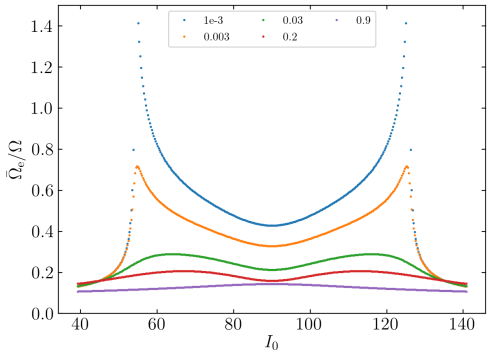

Figure 5. Ratio Ω_e/Ω as a function of I_0 (changing e_{max}) for the close-in regime.

4. ANALYSIS: RESONANCES AND BREAKDOWN OF θ_E CONSERVATION

In the previous section, we assumed the $N \geq 1$ Fourier harmonics in Eq. (18) are negligible when averaging over an LK period. However, when certain resonant conditions are fulfilled, this assumption breaks down. For simplicity, we ignore the effects of GW dissipation in this section, in which case the system is exactly periodic. We again rewrite Eq. (18) in component form in the reference frame where $\hat{\mathbf{z}}' \propto \bar{\mathbf{\Omega}}_e$ (primes are omitted for brevity):

$$\left(\frac{d\hat{\mathbf{S}}}{dt}\right) = \left[\bar{\Omega}_e\hat{\mathbf{z}} + \sum_{N=1}^{\infty} \Omega_{eN}\left(\cos I_N\hat{\mathbf{z}} + \sin I_N\hat{\mathbf{x}}\right)\right] \cos\left(N\Omega t\right) \times \hat{\mathbf{S}}, \tag{45}$$

where I_n is the angle between $\mathbf{\Omega}_{eN}$ and the $\hat{\mathbf{z}}$ axis, and $\Omega = 2\pi/T_{LK}$ is the LK angular frequency. Following a similar procedure to Section 3.1, we obtain a more general form of Eq. (31):

$$\frac{dS_\perp}{dt} = i\left(\bar{\Omega}_e + \Omega_{eN}\cos I_N \cos N\Omega t\right) S_\perp - i\cos\theta \sin I_N \Omega_{eN} \cos N\Omega t. \tag{46}$$

Examining just the second term, we see potential resonances when $\bar{\Omega}_e = N\Omega$. Since, $\bar{\Omega}_e \lesssim \Omega$ for most regions of parameter space (Fig. 5 and 6), we restrict our analysis to resonances with the $N = 1$ component.

A useful measure of the effect of resonances on θ_e conservation is to consider, in the absence of GW dissipation, the Poincaré section of θ_e at eccentricitcy maximum in each LK cycle. When considered across a range of parameters, this shows the ranges of parameter space where θ_e can have substantial oscillations. We choose to vary m_1 and m_2 while holding m_{12} constant, which changes Ω_{SL} but does not change the orbital evolution. The results of this experiment are shown in Figs. 7–9.

An exact calculation of how the resonance produces the θ_e oscillations in Figs. 7 and 8 is beyond the scope of this paper.

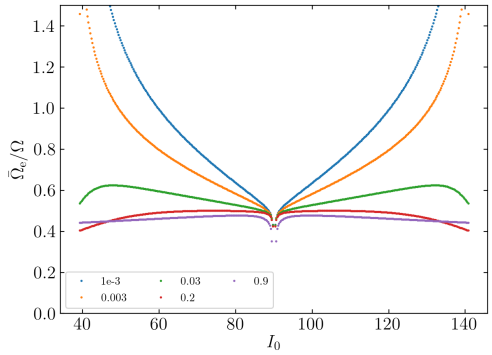

Figure 6. Same as Fig. 5 for the far-out regime.

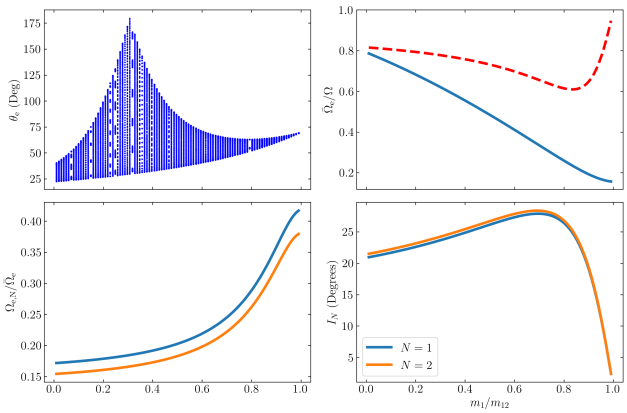

Figure 7. Plots illustrating the effect of the $N = 1$ resonant term on θ_e non-conservation when GW dissipation is ignored. In all plots, m_1 and m_2 are varied while holding their sum m_{12} constant, which changes the spin precession frequency but not the orbital evolution. Top left: the θ_e Poincaré section (taken at eccentricity maxima), where there is clearly significant θ_e excitation around $m_1/m_{12} \approx 0.3$. Top right: (blue) the ratio of $\overline{\Omega}_e/\Omega$ is shown, where Ω is the LK angular frequency, where $\overline{\Omega}_e/\Omega = 1$ is the expected resonance location [Eq. (47), assuming a proportionality factor of 3]; and (red) the heuristic resonance width given by Eq. (47). Comparing to Fig. 8, we see that proximity to the resonance is a necessary condition for θ_e excitation. Bottom panels: magnitude and orientation of the first two Fourier components in Eq. (18). Only the $N = 1$ component is resonant, but the $N = 2$ component is provided for visual comparison.

Instead, we analyze a simpler toy model in Appendix A that suggests θ_e conservation can break when $\left|\overline{\Omega}_e - \Omega\right| \lesssim \Delta\Omega$ for some resonance width $\Delta\Omega$. If we assume the resonance dynamics in the full problem are similar to those in the toy model, we expect a resonance width that scales like

$$\Delta\Omega \propto \Omega_{e1} \sin I_1 . \tag{47}$$

This assumption seems to produce the correct qualitative scaling when examining the top right panels of Figs. 7–9.

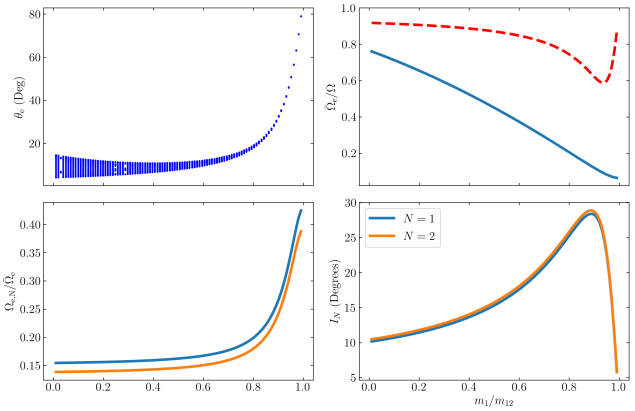

Figure 8. Same as Fig. 7 but for $I_0 = 88°$, which corresponds to a larger e_{max}. We see that $\overline{\Omega}_e$ is significantly farther from the resonance (top left panel) because the $N = 1$ Fourier component is much less misaligned (bottom right panel) which results in much smaller amplitude oscillations in θ_e (top left panel).

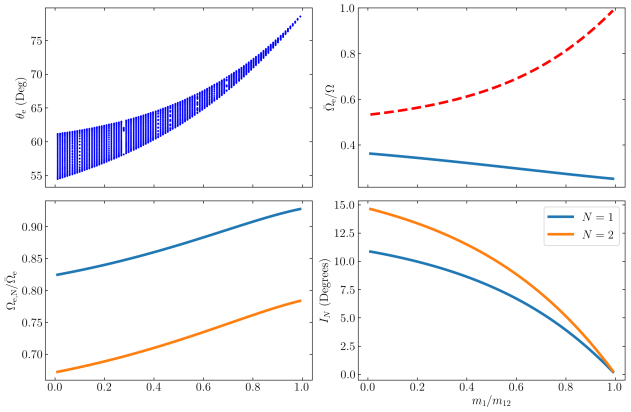

Figure 9. Same as Fig. 7 but for parameters where $\bar{\mathcal{A}} = 1$ in Fig. 1 ($1 - e_0 = 0.0009$, $I_0 = 101°$, $a_0 = 60$ AU). It is clear that again the system is far from resonance.

Eq. (47) implies the following physical parameters encourage breakdown of θ_e conservation:

- $\bar{\mathcal{A}} \simeq 1$. Otherwise, $\mathbf{\Omega}_e$ does not nutate within an LK cycle, and all the $\mathbf{\Omega}_{eN}$ must be aligned with $\overline{\Omega}_e$, implying $I_N \approx 0$.
- $e_{min} \ll e_{max}$. This increases amplitude of nutation in $\mathbf{\Omega}_e$ and therefore increases I_1.
- e_{max} not too extreme. When e_{max} is too large, $\overline{\Omega}_e$ decreases and is farther from the resonance.

LK-driven coalescence causes $\bar{\mathcal{A}}$ to increase on a similar timescale to that of e_{min} increase (see Fig. 1). As such, we conclude that breakdown of θ_e conservation can only occur in systems whose initial conditions are close to satisfying the above criteria.

5. CONCLUSION AND DISCUSSION

Relation between $\theta_{\rm e}$ and $\theta_{\rm sl}^{(\rm f)}$, as a function of I.

The "chaotic" behavior in Paper I is due to the choice of random initial ω, which can change the magnitude of $\overline{\Omega}_{\rm e}$ by around 15–20%. In the resonant scenario, this can greatly change the final outcomes.

REFERENCES

Anderson, K. R., Storch, N. I., & Lai, D. 2016, Monthly Notices of the Royal Astronomical Society, 456, 3671

Liu, B., & Lai, D. 2017, The Astrophysical Journal Letters, 846, L11

—. 2018, The Astrophysical Journal, 863, 68

Peters, P. C. 1964, Physical Review, 136, B1224

Storch, N. I., & Lai, D. 2015, Monthly Notices of the Royal Astronomical Society, 448, 1821

APPENDIX

A. PRECESSION RESONANCE TOY MODEL: RESONANCE WIDTH

In Section 4, we consider how precession about a periodically varying $\mathbf{\Omega}_e$ differs from precession about the mean $\overline{\mathbf{\Omega}}_e$. A toy model for this effect that has nontrivial dynamics and an exact solution is given by

$$\frac{d\hat{\mathbf{S}}}{dt} = \Omega_0 \left[\hat{\mathbf{z}} + \epsilon \left(\sin \omega t \hat{\mathbf{x}} + \cos \omega t \hat{\mathbf{y}}\right)\right] \times \hat{\mathbf{S}}. \tag{A1}$$

This differs from the resonant terms in Eq. (18) since the periodic perturbation here has constant magnitude and varying orientation, while those in Eq. (18) have varying magnitude but remain in the $\hat{\mathbf{x}}$-$\hat{\mathbf{z}}$ plane. Nevertheless, this toy problem gives some insight on the effect of a periodically varying precession axis.

When $\epsilon = 0$ in Eq. (A1), it is clear that $\hat{\mathbf{S}}$ simply precesses about the $\hat{\mathbf{z}}$ axis with frequency Ω_0, and $\cos\theta = \hat{\mathbf{S}} \cdot \hat{\mathbf{z}}$ is constant. However, significant variations in θ can be observed when $\epsilon > 0$. We can go to a rotating reference frame about $\hat{\mathbf{z}}$ where the perturbation is constant (and is chosen to be along the $\hat{\mathbf{x}}'$ axis):

$$\left(\frac{d\hat{\mathbf{S}}}{dt}\right)_{\text{rot}} = \left[(\Omega_0 - \omega)\,\hat{\mathbf{z}} + \Omega_0 \epsilon \hat{\mathbf{x}}'\right] \times \hat{\mathbf{S}}. \tag{A2}$$

It is thus clear that in the rotating reference frame, $\hat{\mathbf{S}}$ precesses about a modified precession axis. When $\Omega_0\epsilon \ll (\Omega_0 - \omega)$, the modified precession axis still lies approximately along $\hat{\mathbf{z}}$, but when $\Omega_0\epsilon \simeq |\Omega_0 - \omega|$ we see that θ will vary significantly over timescales $\sim \epsilon\Omega_0$. Thus, this toy model reveals that Eq. (A1) has a resonance width defined by

$$\left|\frac{\Delta\Omega}{\Omega}\right| \sim \epsilon, \tag{A3}$$

where $\Delta\Omega = \Omega_0 - \omega$, within which θ is not very constant.

Again, while this toy model is an imprecise description of the resonances that are encountered in Eq. (18), it suggests that the relevant resonance width has the scaling proposed in Eq. (47). This is in agreement with further numerical experiments we conducted which are beyond the scope of this paper.